Correlation functions in mixtures with energetically favoured nearest-neighbours of different kind: a size-asymmetric case

O. Patsahan,[1] A. Meyra,[2] and A. Ciach[3]

[1]Institute for Condensed Matter Physics of the National Academy of Sciences of Ukraine,

1 Svientsitskii St., 79011 Lviv, Ukraine

[2]IFLYSIB (UNLP, CONICET), 59 No. 789,

B1900BTE La Plata, Argentina; Depto de Ingenieria Mecánica,

UTN-FRLP, Av. 60 esq. 124, 1900 La Plata, Argentina

[3]Institute of Physical Chemistry, Polish Academy of Sciences,

Kasprzaka 44/52, 01-224 Warszawa, Poland

(Dated: June 18, 2020)

Abstract

Binary mixtures of hard-spheres with different diameters and square-well attraction between different particles are studied by theory and Monte Carlo simulations. In our mesoscopic theory, local fluctuations of the volume fraction of the two components are taken into account. Semi-quantitative agreement between the simulation and theoretical results is obtained, except from very small distances. The correlation functions exhibit exponentially damped oscillations, with the period determined by the interaction potential, and both the amplitude and the correlation length increasing significantly with increasing diameter ratio. Increasing size asymmetry leads also to decreasing fluctuations of the number of the smaller particles in the attractive shell of the bigger ones. For small size asymmetry, the strongest correlations occur for comparable volume fraction of the two components. When the size ratio increases, the maximum of the structure factor moves to a larger volume fraction of the bigger particles, and for the size ratio as large as 4, the maximum goes beyond the accessible range of volume fractions. Our results show that when the neighbourhood of different particles is energetically favoured, the particles are much more uniformly distributed than in the random distribution even at relatively high temperature, especially for large size asymmetry.

1

I. INTRODUCTION

Local structure in simple liquids is determined by packing of hard spheres representing particle cores. Even in the case of spherical shapes, however, the distribution of the particles or molecules can be significantly different when the interactions between them exhibit some competing tendencies. In particular, in the case of electrostatic interactions, repulsion between like charges competes with attraction of opposite charges. At sufficiently low temperature, this competition leads to various ionic crystals in simple salts, as well as to a rich variety of ordered structures in mixtures of oppositely charged colloid particles with different size ratios [1–3]. In the fluid phase, the order can still be present locally, as observed in simulations of ionic liquids (IL) and IL mixtures (ILM) [4], and predicted theoretically [5–11]. The local order can be directly observed near a planar boundary, since the concentration or density profiles are similar to the corresponding correlation functions. Indeed, charge density oscillations in direction perpendicular to the planar boundary have been found in experiments, simulations and theory [12–16]. In directions parallel to the confining plane, either hexagonal or stripe pattern formed by coions is formed in the near-surface layer, and the order extends beyond the first two layers of ions in ILM [15, 17]. Local order in mixtures of colloid particles can be induced by non-coulombic interactions as well, for example by H-bonds formation between different particles [18].

Determination of the local structure in the case of Coulombic interactions by traditional liquid theories is very difficult [6, 19], especially in the case of large size asymmetry. It is easier to determine the structure of the fluid within the density functional theory (DFT) [20] that can very well predict the structure induced by the packing of hard spheres. Unfortunately, in the standard DFT the interactions are taken into account in an expression of the mean-field (MF) type. This expression is inaccurate in a disordered phase with the local structure induced by the competing interactions, and the internal energy in this phase is overestimated [21]. As a result, instead of a disordered phase with strong local order, an ordered phase with long-range charge oscillations with a small amplitude is predicted for a significant part of the phase diagram [7, 22, 23]. A continuous transition to this ordered phase occurs at a λ-surface, where the correlation functions in Fourier representation diverge for a particular wavenumber [7, 10, 23]. Neither this divergency nor the continuous transition exist in reality. This disadvantage is cured in the modified DFT for mixtures, where

the variance of the local volume fraction of the components is taken into account [24]. In Ref.[25], it was shown that the results of the modified DFT agree semiquantitatively with Monte Carlo (MC) simulations for the binary mixture with equal diameters of the particles of the two species. In this work, we consider binary mixtures with different size ratios of the components, and calculate correlation functions within the theory developed in Ref.[24, 25].

Simulations of systems with Coulombic interactions are very difficult too, especially in the case of large size asymmetry [26–28]. It is important to note, however that the periodic arrangement of the particles of the two species is determined by the excess of the energy associated with the density or concentration wave superimposed on the average density or concentration, respectively. As shown in Ref.[24], two types of local order in binary mixtures can occur - either alternating dense and dilute regions are formed, or there are alternating regions rich in the first and in the second component. For the local order formation, the wavenumber corresponding to the largest decrease of the energy compared to the homogeneous state is crucial. For this reason, similar structures are expected for different interaction potentials, if in Fourier representation they assume extrema for the same wavenumbers [29]. We can study model systems that are expected to have similar local structure as systems composed of charged particles. To simplify the simulation studies as much as possible, in this work we consider a model of hard spheres with different diameters of the particles of the two species, and assume a square-well potential between particles of different kind. With such interactions, nearest neighbours of different species are favored energetically over the nearest neighbours of particles of the same species, as in the case of a binary mixture of charged particles.

The objective of our study in this work is twofold. First, we want to determine how the size asymmetry influences the periodic arrangement of particles, when the neighbourhood of different particles is energetically favored. Our second goal is to verify the accuracy of the modified DFT for different size ratios of the particles, and for different thermodynamic states. The theoretical results are compared with Monte Carlo (MC) simulations.

In sec.2, we introduce the model and describe briefly the simulations. In sec. 3, we summarize the theory developed in Ref. [24, 25], and adopt it to the considered model and to the size-asymmetric hard-sphere reference system. In sec.4a, we present theoretical and simulation results for a small size asymmetry. Moderate and large size-asymmetry cases are described in sec.4b and 4c, respectively. The results are summarized in sec.5.

3

II. THE MODEL AND THE SIMULATION METHOD

A. The model

We consider the model binary mixture in which the particles of the same species (like particles) interact through hard-core interactions and the particles of different species interact through the potential $U_{12}(r)$ beyond the hard core. In general, the particles of different species differ in their hard-sphere diameters $\sigma_1 \neq \sigma_2$.

Thus, the pair interaction potentials are as follows:

$$u_{\alpha\alpha}(r) = \begin{cases} \infty, & r < \sigma_\alpha \\ 0, & r \geq \sigma_\alpha \end{cases}, \qquad u_{12}(r) = \begin{cases} \infty, & r < \sigma_{12} \\ U_{12}(r), & r \geq \sigma_{12} \end{cases}, \qquad (1)$$

where $\sigma_{12} = (\sigma_1 + \sigma_2)/2$. For $U_{12}(r)$, we choose the square well potential, which can be presented in the form

$$U_{12}(r) = -\varepsilon\theta(r - 1)\theta(a - r), \qquad (2)$$

where a and r are in σ_{12} units. $a > 1$ is the range of the potential and ε is the interaction strength at contact of the two unlike particles. The Fourier transform of the potential βU_{12} has the form:

$$\beta\tilde{U}_{12}(k) = \frac{4\pi(ak\cos(ak) - k\cos(k) + \sin(k) - \sin(ak))}{k^3}, \qquad (3)$$

where $\beta = 1/(k_B T)$, β is the Boltzmann constant, and the wave-number k is in σ_{12}^{-1} units. The function (3) is shown in Fig. 1 for $a = 1.2$. For $a = 1.2$, the first maximum is at $k = k_0 = 4.062$.

The considered mixture undergoes two types of instability in the MF approximation: the instability (at $k = 0$) connected with the gas-liquid phase separation and the instability (at $k_0 \approx 4.062$) connected with the appearance of local inhomogeneity at the length scale $2\pi/k_0$ [24, 25].

In this work, we want to compare the local structure for small, moderate and large size asymmetry, $\alpha = \sigma_1/\sigma_2$, and choose the following values of the diameter ratio: $\alpha = 0.8, 0.6, 0.25$. The corresponding ratios of the particle volumes, $v_\alpha = \pi\sigma_\alpha^3/6$, are $v_1/v_2 = 0.512, 0.216, 0.015625$, respectively.
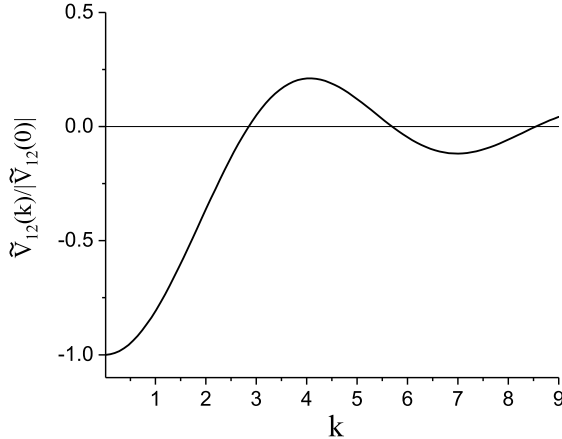
FIG. 1: The Fourier transform of the interaction potential between particles of different kinds (Eq. (2) for $a = 1.2$). The wave-number k is in σ_{12}^{-1} units.

B. The simulations

The binary mixture with $\alpha = 0.8, 0.6, 0.25$ and $a = 1.2\sigma_{12}$, where $\sigma_{12} = (\sigma_1 + \sigma_2)/2$, has been simulated via Monte Carlo technique in the NVT ensemble. $N = N_1 + N_2$ particles (systems I-III in Table I) are placed in a cubic box with periodical boundary conditions applied in the three directions. Interactions between the particles are described in Eqs. (1)–(2). The reference length for the particle size and the simulation box is $\sigma_1 = 1.0$, and the energies are $\epsilon_1 = \epsilon_2 = 0.0$ and $\epsilon_{12} = -1.0$. A cut-off radius, which is the interaction range of the square well potential, depends on σ_2, for that reason it is indicated in Table I. Each system have run 10^7 Monte Carlo steps for equilibration and 10^6 for production.

TABLE I: Simulation details for the systems considered. For systems I–II the size of the simulation box is $20\sigma_1$, but for system III, the box size is $40\sigma_1$. N_1, ζ_1 and N_2, ζ_2 denote the number of particles and the volume fraction of the species 1 and 2, respectively. R_{cut} is the cutoff length in σ_1 units, $\zeta_i = \pi\rho_i\sigma_i^3/6$, $\rho_i = N_i/V$, and $T^* = k_B T/|\epsilon_{12}|$.

Systems	$\alpha = \sigma_1/\sigma_2$	T*	N_1	N_2	ζ_1	ζ_2	R_{cut}
I	0.8	0.1	2597	1799	0.17	0.23	1.35
II	0.6	0.1	3514	886	0.23	0.27	1.6
III	0.25	0.6	15890	516	0.13	0.27	3.0

III. THEORY

A. Brief summary of the DFT for inhomogeneous mixtures

In the case of size asymmetry, the number density of smaller particles can be larger than the number density of the big ones, but the volume occupied by them can be significantly smaller. For this reason, the theory developed in Ref. [24] is based on the local volume fractions, $\zeta_\alpha(\mathbf{r}) < 1$, where in the binary mixture $\alpha = 1, 2$. We are interested in the correlation functions in the disordered phase,

$$G_{\alpha\beta}(\mathbf{r}) = \langle \Delta\zeta_\alpha(\mathbf{r}_0)\Delta\zeta_\beta(\mathbf{r}+\mathbf{r}_0)\rangle, \tag{4}$$

where $\Delta\zeta_\alpha(\mathbf{r}) = \zeta_\alpha(\mathbf{r}) - \bar{\zeta}_\alpha$, and $\bar{\zeta}_\alpha$ is the average volume fraction of the species α in the disordered phase. The matrix $\mathbf{G}$ with the elements defined in (4) satisfies the analog of the Ornstein-Zernicke equation, $\mathbf{G} = \mathbf{C}^{-1}$, where the inverse correlation functions $\tilde{C}_{\alpha\beta}(\mathbf{r}_1, \mathbf{r}_2)$ (related to the direct correlation functions) are the second functional derivatives with respect to $\zeta_\alpha(\mathbf{r}_1)$ and $\zeta_\beta(\mathbf{r}_2)$ of the functional

$$\beta F[\zeta_1, \zeta_2] = \beta\Omega_{co}[\zeta_1, \zeta_2] - \ln\left[\int D\phi_1 \int D\phi_2 e^{-\beta H_{fluc}}\right], \tag{5}$$

where

$$H_{fluc}[\zeta_1, \zeta_2|\phi_1, \phi_2] = \Omega_{co}[\zeta_1 + \phi_1, \zeta_2 + \phi_2] - \Omega_{co}[\zeta_1, \zeta_2],$$

and $\Omega_{co}[\zeta_1, \zeta_2]$ is the grand potential with the local volume fractions constrained to have the fixed forms. We assume

$$\Omega_{co} = \frac{1}{2}\int d\mathbf{r}_1 \int d\mathbf{r}_2 V_{\alpha\beta}(|\mathbf{r}_1 - \mathbf{r}_2|)\zeta_\alpha(\mathbf{r}_1)\zeta_\beta(\mathbf{r}_2) - TS - \mu_\alpha N_\alpha,$$

where $V_{\alpha\beta}(r) = U_{\alpha\beta}(r)/(v_\alpha v_\beta)$ is the interaction potential (in appropriate units) between the species α and β separated by the distance r, the entropy S satisfies the relation $-TS = \int f_h(\zeta_1(\mathbf{r}), \zeta_2(\mathbf{r}))d\mathbf{r}$, where f_h is the free-energy density of the hard-core reference system in the local-density approximation, and μ_α, N_α are the chemical potential and the number of particles of the species α, respectively. $\phi_\alpha(\mathbf{r})$ is the local fluctuation of the volume fraction of the component α.

In MF, the second term on the RHS of Eq.(5) is neglected. In the lowest-order nontrivial approximation beyond MF [24],

$$\tilde{C}_{\alpha\beta}(k) = \beta\tilde{V}_{\alpha\beta}(k) + A_{\alpha\beta} + \frac{A_{\alpha\beta\gamma\delta}}{2}\mathcal{G}_{\gamma\delta}, \tag{6}$$

where $\tilde{f}(k)$ denotes the function f in Fourier representation, and the summation convention is used. In the above equation,

$$A_{\alpha_1....\alpha_j} = \frac{\partial^j \beta f_h(\zeta_1, \zeta_2)}{\partial \zeta_{\alpha_1}...\partial \zeta_{\alpha_j}}, \tag{7}$$

with $\alpha_i = 1, 2$. Note that in this approximation, the dependence of $\tilde{C}_{\alpha\beta}(k)$ on k comes only from $\beta \tilde{V}_{\alpha\beta}(k)$. The last term in Eq.(6) is the fluctuation contribution, and comes from the last term in (5) in the Brazovskii-type approximation [30]. Here, $\mathcal{G}_{\gamma\delta}$ denotes the integral

$$\mathcal{G}_{\gamma\delta} = \int \frac{d\mathbf{k}}{(2\pi)^3} \tilde{G}_{\gamma\delta}(k). \tag{8}$$

Eqs.(6)-(8) have to be solved self-consistently. In general, it is a nontrivial task.

We focus on the disordered inhomogeneous phase and assume that the inhomogeneities occur on a well-defined length scale. In such a case, the peak of $\tilde{G}_{\gamma\delta}(k)$ is high and narrow. For functions with a high, narrow peak, the main contribution to the integral comes from the vicinity of the maximum. We assume that the maximum of all the integrands in (8) is very close to the minimum at $k = k_0$ of $\det \tilde{\mathbf{C}}(k)$, and we make the approximation

$$\mathcal{G}_{\alpha\beta} = [\tilde{C}_{\alpha\beta}(k_0)]\mathcal{G}, \tag{9}$$

where $[\tilde{C}_{\alpha\alpha}(k)] = \tilde{C}_{\beta\beta}(k)$ and $[\tilde{C}_{\alpha\beta}(k)] = -\tilde{C}_{\alpha\beta}(k)$ for $\alpha \neq \beta$, and

$$\mathcal{G} = \int \frac{d\mathbf{k}}{(2\pi)^3} \frac{1}{\det \tilde{\mathbf{C}}(k)}. \tag{10}$$

Near the minimum at k_0, we have the approximation

$$\det \tilde{\mathbf{C}}(k) = D_0 + \frac{\beta \tilde{W}''(k_0)}{2}(k - k_0)^2 + ... \tag{11}$$

where $\tilde{W}''(k_0)$ depends on the interaction potentials, and

$$D_0 = \det \tilde{\mathbf{C}}(k_0). \tag{12}$$

From the approximation (11) and (10), we obtain [24, 31]

$$\mathcal{G} \approx \frac{k_0^2}{\pi\sqrt{2\beta\tilde{W}''(k_0)D_0}}. \tag{13}$$

With all the above assumptions, the problem reduces to determination of the minimum of $\det \tilde{\mathbf{C}}(k)$, and to a solution of 3 algebraic equations for $\tilde{C}_{\alpha\beta}(k_0)$ (see Eq.(6) for $k = k_0$), because

$$\tilde{C}_{\alpha\beta}(k) = \tilde{C}_{\alpha\beta}(k_0) + \beta(\tilde{V}_{\alpha\beta}(k) - \tilde{V}_{\alpha\beta}(k_0)). \tag{14}$$

7

B. Correlation functions in the considered model

For the model (1)-(2), the closed set of 4 equations for the unknowns k_0 and $\tilde{C}_{\alpha\beta}(k_0)$ takes the form

$$\tilde{V}'_{12}(k_0) = 0, \tag{15}$$

$$\tilde{C}_{11}(k_0) = A_{11} + \frac{k_0^2}{2\pi\sqrt{2\beta\tilde{W}''(k_0)D_0}}\left[A_{1111}\tilde{C}_{22}(k_0) - 2A_{1112}\tilde{C}_{12}(k_0) + A_{1122}\tilde{C}_{11}(k_0)\right], \tag{16}$$

$$\tilde{C}_{22}(k_0) = A_{22} + \frac{k_0^2}{2\pi\sqrt{2\beta\tilde{W}''(k_0)D_0}}\left[A_{1122}\tilde{C}_{22}(k_0) - 2A_{1222}\tilde{C}_{12}(k_0) + A_{2222}\tilde{C}_{11}(k_0)\right], \tag{17}$$

$$\tilde{C}_{12}(k_0) = \beta\tilde{V}_{12}(k_0) + A_{12} + \frac{k_0^2}{2\pi\sqrt{2\beta\tilde{W}''(k_0)D_0}}\left[A_{1112}\tilde{C}_{22}(k_0) - 2A_{1122}\tilde{C}_{12}(k_0)\right.$$
$$\left. + A_{1222}\tilde{C}_{11}(k_0)\right], \tag{18}$$

where

$$\tilde{W}''(k_0) = -2\tilde{V}''_{12}(k_0)\tilde{C}_{12}(k_0), \tag{19}$$

and we denote by $'$ ($''$) the first (second)-order derivative of $\tilde{V}_{12}(k)$ with respect to the wave number k. Note that the minimum of $\det\tilde{\mathbf{C}}(k)$ corresponds to the maximum of $\tilde{V}_{12}(k)$.

Once Eqs.(15)-(18) are solved, the correlation functions $\tilde{C}_{\alpha\beta}(k)$ can be obtained from Eq.(14). Finally, the interaction potential $\tilde{V}_{12}(k)$ (an even function of k) is approximated as follows:

$$\tilde{V}_{12}(k) \approx \tilde{V}_{12}(k_0) + \frac{V''_{12}(k_0)}{8k_0^2}(k^2 - k_0^2)^2. \tag{20}$$

To calculate $\tilde{G}_{\alpha\beta}(k)$ in the Brazovskii-type approximation, we solve Eqs (16)-(18) with respect to $\tilde{C}_{\alpha\beta}(k_0)$ and from $\mathbf{G} = \mathbf{C}^{-1}$, we obtain

$$\tilde{G}_{11}(k) = \frac{\tilde{C}_{22}(k_0)}{D(k)}, \qquad \tilde{G}_{22}(k) = \frac{\tilde{C}_{11}(k_0)}{D(k)}, \tag{21}$$

$$\tilde{G}_{12}(k) = -\frac{\tilde{C}_{12}(k_0) + \beta\Delta\tilde{V}_{12}(k)}{D(k)}, \tag{22}$$

where

$$D(k) = \tilde{C}_{11}(k_0)\tilde{C}_{22}(k_0) - (\tilde{C}_{12}(k_0) + \beta\Delta\tilde{V}_{12}(k))^2, \tag{23}$$

and $\Delta\tilde{V}_{12}(k) = \tilde{V}_{12}(k) - \tilde{V}_{12}(k_0) \approx \frac{V''_{12}(k_0)}{8k_0^2}(k^2 - k_0^2)^2$ (see Eq. (20)).

8

In MF, the correlation functions are given by Eqs.(21)-(23), but with $\tilde{C}_{\alpha\alpha}(k)$ approximated by $A_{\alpha\alpha}$, and $\tilde{C}_{12}(k)$ approximated by $A_{12} + \beta\tilde{V}_{12}(k)$. The correlation functions diverge for vanishing denominator in (21)-(22). From the MF equation $D(k) = A_{11}A_{22} - (A_{12} + \beta\tilde{V}_{12}(k))^2 = 0$ one can get the expressions for both the gas-liquid spinodals and the λ-surfaces:

$$T^*_{sp} = - \left(\frac{3}{4\pi}\right)^2 \frac{(1+\alpha)^6}{\alpha^3} \frac{\tilde{V}_{12}(0)}{\sqrt{A_{11}A_{22}} + A_{12}}, \tag{24}$$

$$T^*_\lambda = \left(\frac{3}{4\pi}\right)^2 \frac{(1+\alpha)^6}{\alpha^3} \frac{\tilde{V}_{12}(k_0)}{\sqrt{A_{11}A_{22}} - A_{12}}, \tag{25}$$

where $T^* = k_B T/\varepsilon$, and

$$\tilde{V}_{12}(k_0 = 0) = -\frac{4}{3}\pi(a^3 - 1), \qquad \tilde{V}_{12}(k_0 = 4.062, a = 1.2) \simeq 0.644. \tag{26}$$

C. Free energy for a mixture of hard-spheres with unequal diameters

We present the free-energy density of the reference system as follows:

$$f_h(\zeta_1, \zeta_2) = \zeta_1 \ln \zeta_1 + \zeta_2 \ln \zeta_2 + f_{ex}(\zeta_1, \zeta_2), \tag{27}$$

where in the Carnahan-Starling approximation $f_{ex}(\zeta_1, \zeta_2)$ has the form [32]:

$$f_{ex}(\zeta_1, \zeta_2) = \frac{6}{\pi}\left(\frac{1+\alpha}{2\alpha}\right)^3 (\zeta_1 + \alpha^3\zeta_2) \left[-1 - \frac{3}{2}(1 - y_1 + y_2 + y_3)\right.$$
$$\left. + \frac{3y_2 + 2y_3}{1 - \zeta} + \frac{3}{2}\frac{(1 - y_1 - y_2 - y_3/3)}{(1 - \zeta)^2} + (y_3 - 1)\ln(1 - \zeta)\right], \tag{28}$$

with

$$y_1 = \Delta_{12}\frac{1+\alpha}{\sqrt{\alpha}}, \qquad y_2 = \Delta_{12}\frac{\zeta_1 + \alpha\zeta_2}{\sqrt{\alpha}\zeta}, \qquad y_3 = \frac{(\zeta_1 + \alpha\zeta_2)^3}{(\zeta_1 + \alpha^3\zeta_2)\zeta^2}, \tag{29}$$

$$\Delta_{12} = \frac{\zeta_1\zeta_2(\alpha - 1)^2\sqrt{\alpha}}{(\zeta_1 + \alpha^3\zeta_2)\zeta}, \tag{30}$$

and $\zeta = \zeta_1 + \zeta_2$ ($\zeta_\alpha = \pi\rho_\alpha\sigma_\alpha^3/6$). For $\alpha = 1$, $f_{ex}(\zeta_1, \zeta_2)$ reduces to the free energy density for a one-component case $f_{ex}(\zeta)$.

Introducing the concentration of the 2nd species, $x = \rho_2/\rho$, we can present the packing fractions ζ_1 and ζ_2 as follows:

$$\zeta_1 = \frac{(1-x)\alpha^3\zeta}{x + (1-x)\alpha^3}, \qquad \zeta_2 = \frac{x\zeta}{x + (1-x)\alpha^3}. \tag{31}$$

9

Alternatively, the fraction of the volume occupied by the larger particles, $c = \zeta_2/\zeta$, can be considered. Using Eqs. (27)-(30), one can get explicit expressions for $A_{\alpha\beta}$ and $A_{\alpha\beta\gamma\nu}$. For the fixed diameter ratio α, they are functions of both the total packing fraction ζ and either the concentration x, or c.

IV. RESULTS

A. Case $\alpha = 0.8$

1. Theoretical results

We start with the case of small size asymmetry $\alpha = 0.8$ ($\sigma_2 = 1.25\sigma_1$). In Fig. 2, we present the T^*-ζ-plots of the MF boundaries of the stability of the disordered phase (see Eqs. (24)-(25)) for a set of fixed concentrations. In Fig. 2, the curves with maxima are the gas-liquid spinodals, while the λ-lines are presented as straight lines. As one can see, the dependence of T^* on the concentration at the fixed ζ is nonmonotonic (for both types of instability). This is in contrast to the case of a size-symmetric mixture [25].
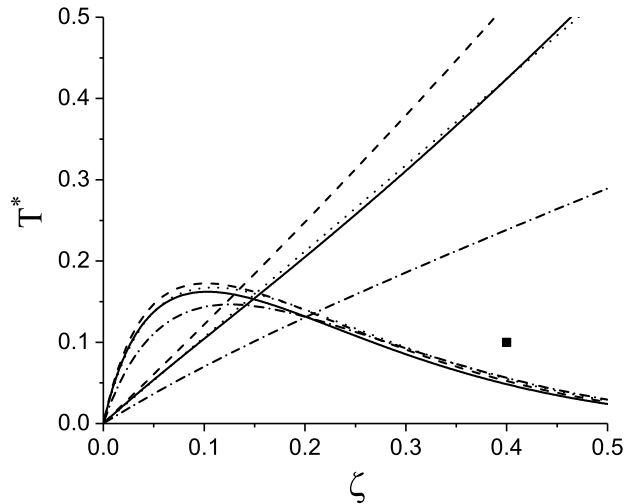
FIG. 2: Gas-liquid spinodals and λ-lines for the model (2) at $a = 1.2$ and $\alpha = 0.8$ for different concentrations. Solid lines: $c = 0.33$ ($x = 0.2$), dashed lines: $c = 0.57$ ($x = 0.4$), dotted lines: $c = 0.75$ ($x = 0.6$), and dash-dotted lines: $c = 0.89$ ($x = 0.8$). The filled square denotes the thermodynamic state located below the λ-surface but above the gas-liquid spinodal, for which the correlation functions are shown in Fig.4 (see text for more details).

10

First, we calculate the MF correlation functions in Fourier representation above the λ-surface. The corresponding correlation functions $\tilde{G}_{\alpha\beta}(k)$ are shown in Fig. 3 (panel a) for $T^* = 0.52$, $\zeta = 0.4$ and $c = 0.57$. The maximum (minimum) of $\tilde{G}_{\alpha\beta}(k)$ corresponds to the maximum of the interaction potential $\tilde{V}_{12}(k)$ and it is located at $k = k_0$ (see Fig. 1).
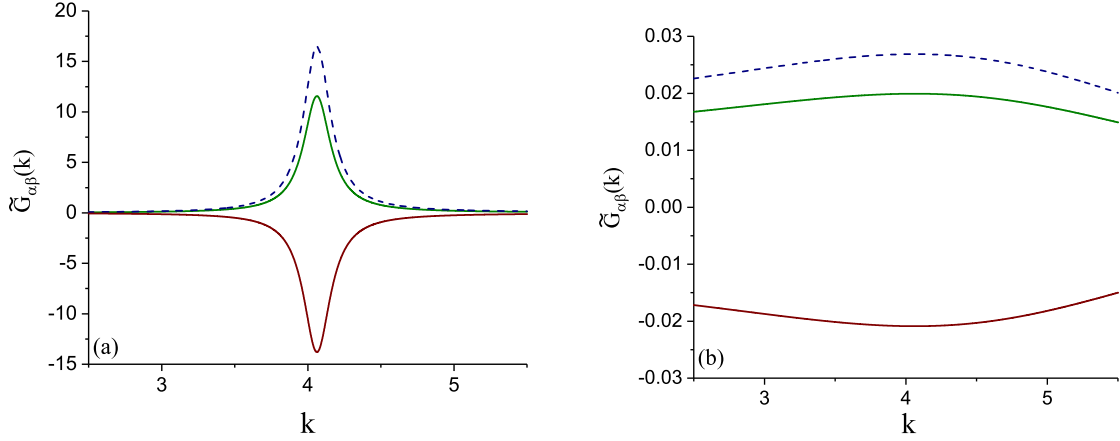

FIG. 3: (Colour online) Correlation functions $\tilde{G}_{\alpha\beta}(k)$ for $\alpha = 0.8$ in MF approximation (panel a) and with the effect of fluctuations taken into account (panel b) for the thermodynamic state above the λ-surface: $T^* = 0.52$, $\zeta = 0.4$ and $c = 0.57$ ($x = 0.4$). Upper solid lines: $\tilde{G}_{11}(k)$, dashed lines: $\tilde{G}_{22}(k)$, and lower solid lines: $\tilde{G}_{12}(k)$.
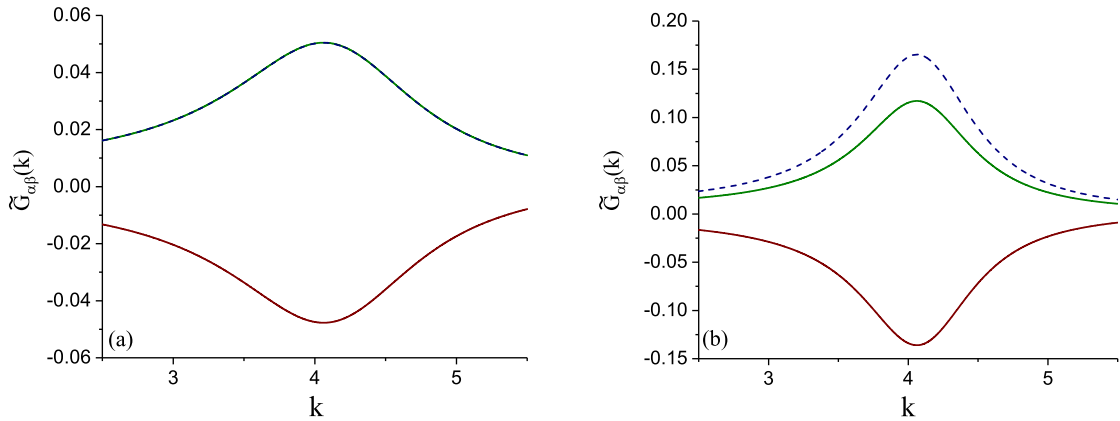

FIG. 4: (Colour online) Correlation functions in Fourier representation for $\alpha = 0.8$ with the effect of fluctuations taken into account. Upper solid lines: $\tilde{G}_{11}(k)$, dashed lines: $\tilde{G}_{22}(k)$ and lower solid lines: $\tilde{G}_{12}(k)$. $T^* = 0.1$, $\zeta = 0.4$ and $c = 0.33$ (panel a), $c = 0.57$ (panel b).

Now, we go beyond MF and calculate the correlation functions in Fourier representation, taking into account the effect of fluctuations. We fix the total volume fraction at $\zeta = 0.4$

11

TABLE II: The decay length α_0^{-1} and the period of oscillations $\lambda = 2\pi/\alpha_1$ of the pair correlation functions $G_{\alpha\beta}(r)$ (Eq. (32)) depending on the total number density ζ for fixed values of the size asymmetry ratio α, temperature T^* and concentration c. $T^* = k_B T/|\epsilon_{12}|$, α_0 and α_1 are in σ_{12}^{-1} units

$\alpha = \sigma_1/\sigma_2$	T^*	$c = \zeta_2/\zeta$	ζ	α_0	α_1	α_0^{-1}	$2\pi/\alpha_1$
0.8	0.1	0.57	0.4	0.4891	4.092	2.044	1.536
0.8	0.1	0.57	0.45	0.359	4.078	2.785	1.541
0.8	0.1	0.57	0.5	0.267	4.071	3.750	1.543
0.6	0.1	0.54	0.4	0.376	4.080	2.657	1.540
0.6	0.1	0.54	0.45	0.265	4.071	3.775	1.543
0.6	0.1	0.54	0.5	0.189	4.067	5.290	1.545
0.25	0.6	0.67	0.3	1.306	4.267	0.766	1.472
0.25	0.6	0.67	0.35	0.676	4.118	1.478	1.526
0.25	0.6	0.67	0.4	0.112	4.064	8.928	1.546

and consider the temperatures above and below the λ-surface. In Fig. 3 (panel b), $\tilde{G}_{\alpha\beta}(k)$ are compared with the MF result for the same values of temperature, total volume fraction, and concentration. It is seen that the maxima (minimum) of the correlation functions for the temperature above the λ-surface become very flat when the fluctuations are taken into account and k_0 is not shifted in this case. In Fig 4, we present the results for $\tilde{G}_{\alpha\beta}(k)$ for the temperature $T^* = 0.1$, the total volume fraction $\zeta = 0.4$ and for two values of the bigger particle concentration: $c = 0.33$ (panel a) and $c = 0.57$ (panel b). These thermodynamic states are located below the λ-surface and beyond the MF gas-liquid spinodal (see the state denoted by the filled square in Fig. 2). It should be noted that the correlation functions $\tilde{G}_{\alpha\beta}(k)$ at k_0 take their maximal (minimal) values for the concentration $c \approx 0.57$. For $c = 0.33$, $\tilde{G}_{11}(k)$ and $\tilde{G}_{22}(k)$ coincide; the maximum of $\tilde{G}_{11}(k)$ becomes larger (smaller) than the maximum of $\tilde{G}_{22}(k_0)$ for $c < 0.33$ ($c > 0.33$).

The correlation functions in real-space representation, obtained by the inverse Fourier transformation of $\tilde{G}_{\alpha\beta}(k)$, are shown in Fig.5 for $T^* = 0.1$, $\zeta = 0.4$ and $c = 0.57$. It is seen from Fig. 5 that $G_{\alpha\beta}(r)$ show exponentially damped oscillatory behavior with the period of damped oscillations $\lambda/\sigma_{12} \simeq 1.54$ which is close to $2\pi/k_0 \simeq 1.547$. In addition, $G_{12}(r)$ and

$G_{\alpha\alpha}(r)$ exhibit their extrema at the same values of r and the maximum of $G_{\alpha\alpha}(r)$ coincides with the minimum of $G_{12}(r)$. In general, $G_{\alpha\beta}(r)$ for $r \gg 1$ are described by the functions [6]

$$G_{\alpha\beta}(r) = A_{\alpha\beta}e^{-\alpha_0 r}\sin(\alpha_1 r)/r. \qquad (32)$$

In (32), α_0 and α_1 are the imaginary and real parts of the leading order pole of $\tilde{G}_{\alpha\beta}(k)$ which is determined as the complex root $k = \alpha_1 \pm i\alpha_0$ of the equation $D(k) = 0$ (see Eq. (23)) having the smallest imaginary part. All the $\tilde{G}_{\alpha\beta}(k)$ have the same pole structure and the same α_1 and α_0. For the above-mentioned thermodynamic state, we get $\alpha_0\sigma_{12} \simeq 0.49$, $\alpha_1\sigma_{12} \simeq 4.1$, $A_{11} \simeq 0.038$, $A_{22} \simeq 0.0525$, and $A_{12} \simeq -0.045$. It should be noted that the amplitudes $A_{\alpha\beta}$ satisfy the rule

$$A_{12}^2 = A_{11}A_{22}, \qquad (33)$$
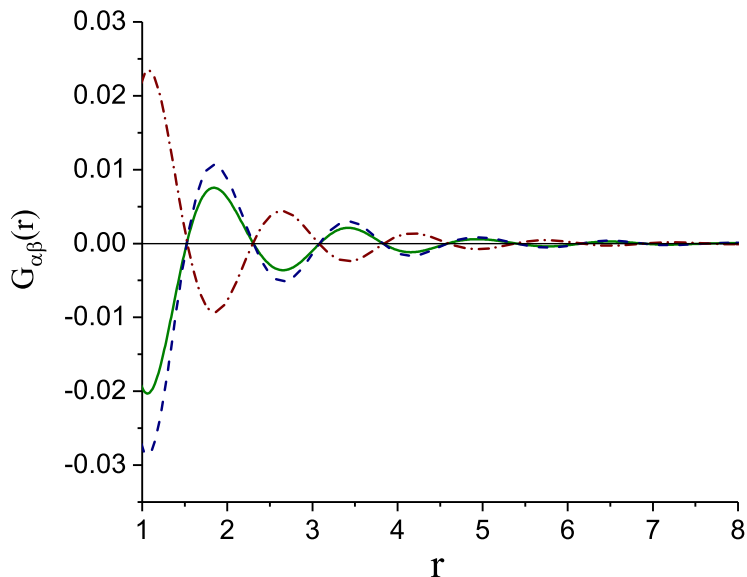
derived from general considerations [33].

FIG. 5: (Colour online) Case $\alpha = 0.8$. Correlation functions in real space for $T^* = 0.1$, $\zeta = 0.4$ and $c = 0.57$ with the effect of fluctuations taken into account. $G_{11}(r)$ (solid line), $G_{22}(r)$ (dashed line) and $G_{12}(r)$ (dash-dotted line). r is in σ_{12} units.

The decay length, α_0^{-1}, and the period of oscillations, $\lambda = 2\pi/\alpha_1$, are shown in Fig. 6 as functions of the concentration c for the total volume fraction $\zeta = 0.4$ and for two values of temperature, $T^* = 0.082$ and 0.1. As it is seen, both α_0^{-1} and λ exhibit a nonmonotonic behavior with the concentration: α_0^{-1} has a pronounced maximum for $c \simeq 0.57$, whereas
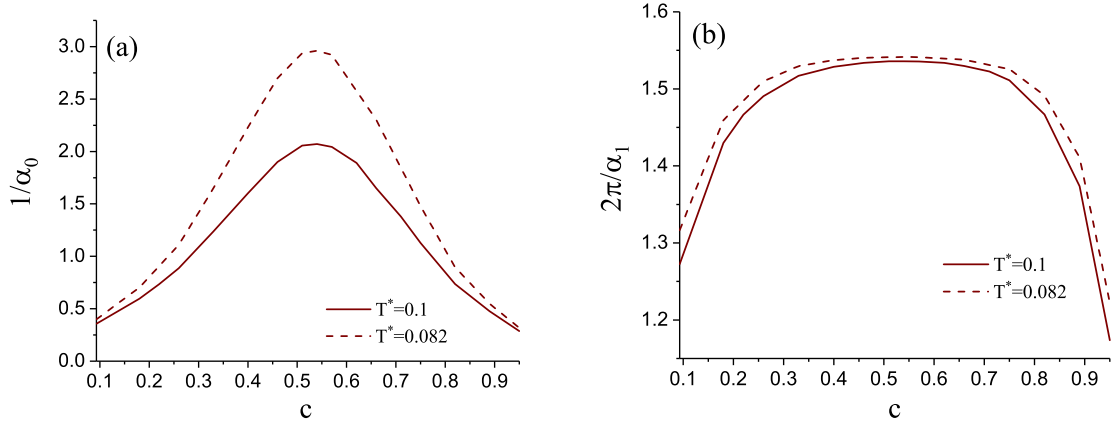
FIG. 6: The decay length α_0^{-1} (panel a) and the period of oscillations $\lambda = 2\pi/\alpha_1$ (panel b) of the correlation functions $G_{\alpha\beta}$ for $\alpha = 0.8$ as functions of the concentration for two values of temperature: $T^* = 0.082$ (dashed line) and $T^* = 0.1$ (solid line). α_0 and α_1 are in units of σ_{12}^{-1}.

λ exhibits a wide, flat maximum region. The decay length increases noticeably when the temperature decreases, while the temperature dependence of λ is very weak. Similarly, α_0^{-1} varies quite rapidly on increasing (decreasing) the total volume fraction, whereas λ changes only very slightly (see Table II).

2. Simulation results

The details of simulations of a binary mixture with $\alpha = 0.8$ are given in Table I (see System I).

In Fig. 7, the pair distribution functions $g_{\alpha\beta} = \frac{G_{\alpha\beta}}{\zeta_\alpha \zeta_\beta} + 1$ and a representative configuration are presented for $T^* = 0.1$, $\zeta = 0.4$ and $c = 0.57$. On the snapshot, darker (red) colour is used to denote bigger particles and lighter (cyan) colour is used for smaller particles. One can see that smaller and bigger particles are located next to each other.

For the pair distribution functions $g_{\alpha\beta}(r)$, an oscillatory decay with the period of the damped oscillations $\lambda \approx 1.1\sigma_1 \simeq \sigma_{12}$ can be seen (Fig. 7). Simultaneously, the minima of $g_{12}(r)$ more or less coincide with the maxima of $g_{\alpha\alpha}(r)$ only for large distances. This deviations from the theoretical predictions can be related to the effect of the hard sphere packing which becomes important for the large density. In order to separate this effect, we
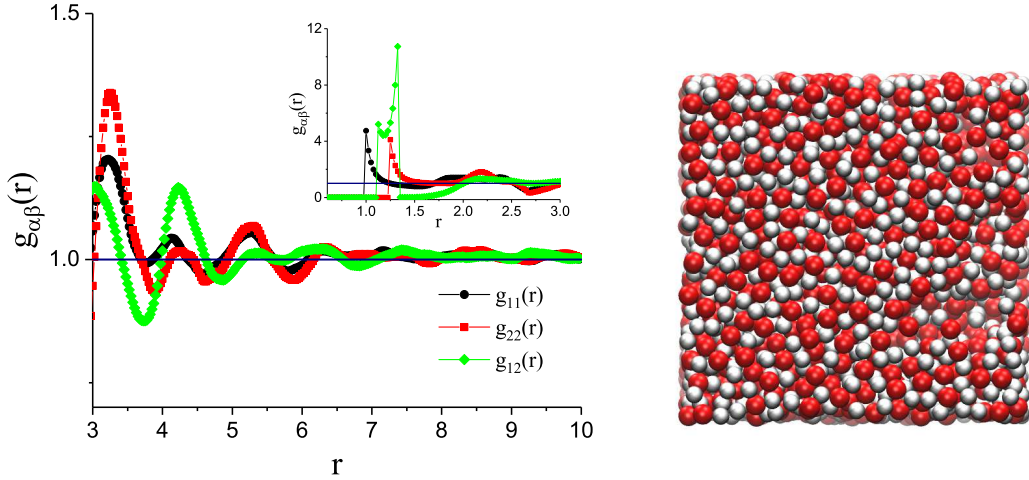
14

FIG. 7: (Colour online) Pair distribution functions and a representative configuration of the model with $\alpha = 0.8$ for $T^* = 0.1$, total volume fraction $\zeta = 0.4$ and concentration $c = 0.57$. r is in σ_1 units.
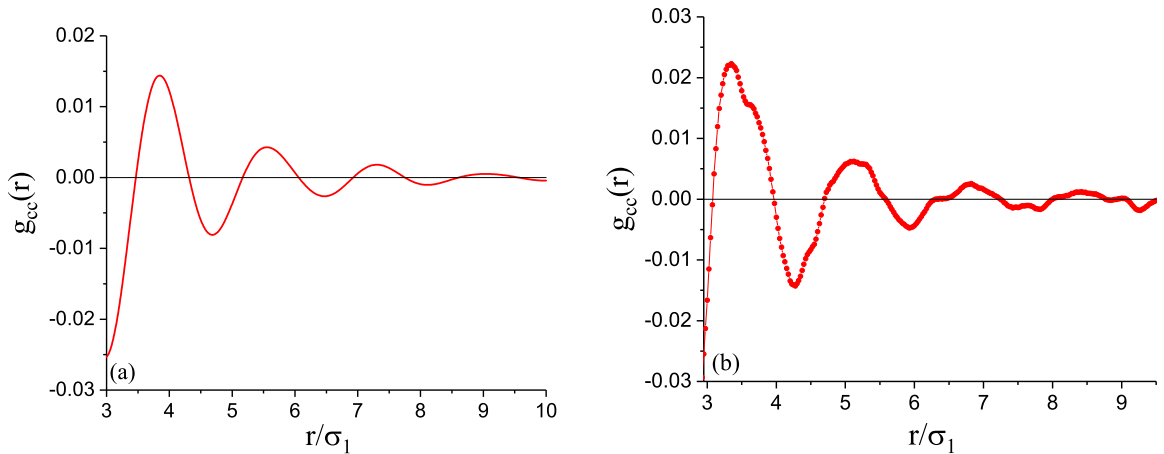

FIG. 8: Concentration-concentration distribution function $g_{cc}(r)$ for $\alpha = 0.8$. Panel a: theoretical results and panel b: results of simulations. $T^* = 0.1$, $\zeta = 0.4$ and $c = 0.57$. r is in σ_1 units.

calculate the concentration-concentration distribution functions [34]

$$g_{cc}(r) = x^2(1-x)^2 \left[g_{11}(r) + g_{22}(r) - 2g_{12}(r) \right].$$

In Fig. 8, we present $g_{cc}(r)$ obtained from the theory and from the simulations for $T^* = 0.1$, $\zeta = 0.4$ and $c = 0.57$. It is seen that the theoretical results are in good agreement with the simulation findings. The theory and simulations show oscillatory decay and the periods of damped oscillations which are close to each other. The maxima and minima of
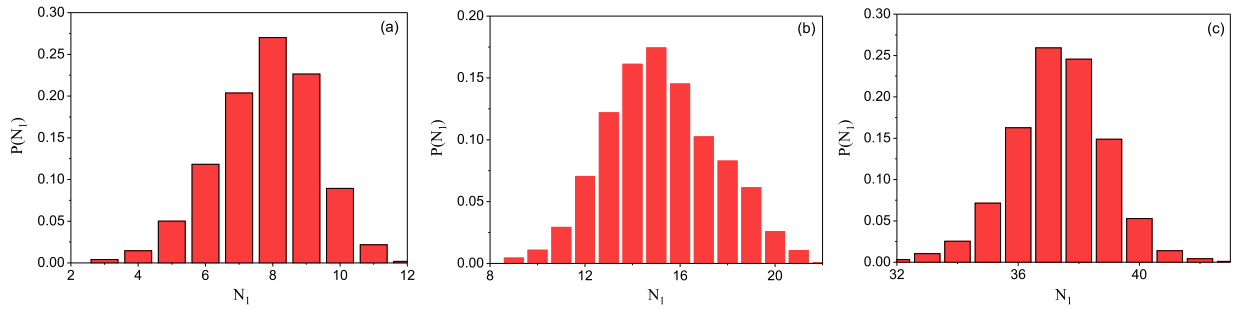
the oscillations occur for similar r.

FIG. 9: Histograms of the probability to find N_1 smaller particles at a distance $\sigma_{12} < r < 1.2\sigma_{12}$ from the center of a bigger particle. Panel a: $\alpha = 0.8$ ($T^* = 0.1$, $\zeta = 0.4$, $c = 0.57$), panel b: $\alpha = 0.6$ ($T^* = 0.1$, $\zeta = 0.5$, $c = 0.54$) and panel c: $\alpha = 0.25$ ($T^* = 0.6$, $\zeta = 0.4$, $c = 0.67$).

The theory summarized in sec. 3a can be valid only for $r \gg 1$, i.e. it allows to study ordering on the mesoscopic length scale. It is interesting, however, to analyze the local ordering of the smaller particles in the attractive shell of the bigger one. The degree of order is not only described by the pair distribution function that tells about the average number of the particles at a given distance from the considered one, but also by the fluctuation of this number. This information can be inferred from simulations by determining the probability distribution of finding N_1 smaller particles at a distance $\sigma_{12} < r < 1.2\sigma_{12}$ from the center of the bigger one (corresponding to the attractive shell).

The histograms $P(N_1)$ of the probability of finding N_1 smaller particles at a distance $\sigma_{12} < r < 1.2\sigma_{12}$ from the center of a bigger particle are presented in Fig. 9. The results for $\alpha = 0.8$ (panel a) indicate that the bigger particle is most likely to have 8 nearest-neighbours. This implies that the periodic ordering resembling ionic crystal structure can occur on the mesoscopic length scale. However, fluctuations of N_1 in the attractive shell are quite large.

B. Case $\alpha = 0.6$

1. Theoretical results

Now we consider the case of a moderate size-asymmetry, $\alpha = 0.6$ ($\sigma_2 \simeq 1.7\sigma_1$). For this mixture, the MF boundaries of stability for the fixed values of concentration are presented in Fig. 10. As for $\alpha = 0.8$, the dependence of T^* on the bigger particle concentration for

fixed ζ is nonmonotonic. Now, the λ-lines are no longer straight lines for lower values of concentration.
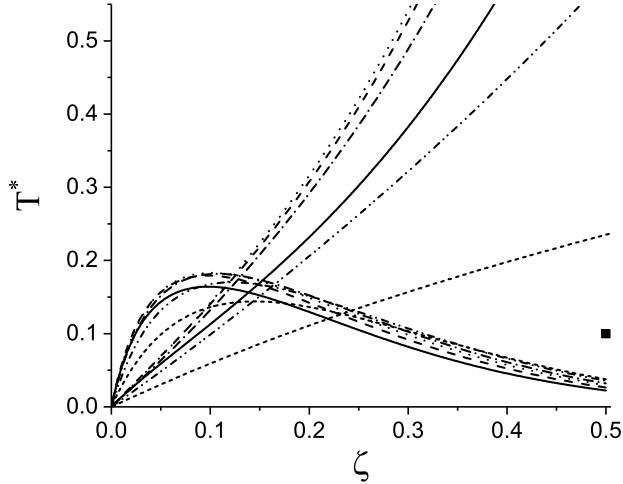

FIG. 10: Gas-liquid spinodals and λ-lines for the model (2) at $a = 1.2$ and $\alpha = 0.6$ for different concentrations. Solid lines: $c = 0.34$ ($x = 0.1$), dashed lines: $c = 0.54$ ($x = 0.2$), dotted lines: $c = 0.67$ ($x = 0.3$), dash-dotted lines: $c = 0.76$ ($x = 0.4$), dash-dot-dotted lines: $c = 0.87$ ($x = 0.6$), and short-dashed lines: $c = 0.95$ ($x = 0.8$). The filled square denotes the thermodynamic state located below the λ-surface but above the gas-liquid spinodal (see text for details).

We focus on the region below the λ-surface and calculate the correlation functions in Fourier representation taking into account fluctuations (Eqs. (21)-(23) complemented by Eqs. (16)-(18) for $\tilde{C}_{\alpha\beta}(k_0)$). We consider the thermodynamic state denoted by the filled square in Fig. 10. The results for $T^* = 0.1$, $\zeta = 0.5$ and for two values of concentration, $c = 0.34$ and $c = 0.54$, are presented in Fig. 11. For $c > 0.1$, a maximum of $\tilde{G}_{22}(k)$ is higher than a maximum of $\tilde{G}_{11}(k)$. The opposite situation is observed for $c < 0.1$.

The correlation functions in real space for $T^* = 0.1$, $\zeta = 0.5$ and $c = 0.54$ are presented in Fig. 12. As for $\alpha = 0.8$, $G_{\alpha\beta}(r)$ have the form (32) and show exponentially damped oscillatory decay with the period of damped oscillations $\lambda/\sigma_{12} \simeq 1.54$. A maximum of $G_{\alpha\alpha}(r)$ coincides with a minimum of $G_{12}(r)$. In the present case, however, the oscillations are more long-ranged. For the considered thermodynamic state, $\alpha_0\sigma_{12} \simeq 0.19$, $\alpha_1\sigma_{12} \simeq 4.1$, $A_{11} \simeq 0.075$, $A_{22} \simeq 0.13$, and $A_{12} \simeq -0.096$. As for $\alpha = 0.8$, the amplitudes satisfy the rule (33).

In Fig. 13, the decay length α_0^{-1} and the period of damped oscillations λ are presented as functions of the concentration c for fixed total volume fraction ($\zeta = 0.5$) and for two values
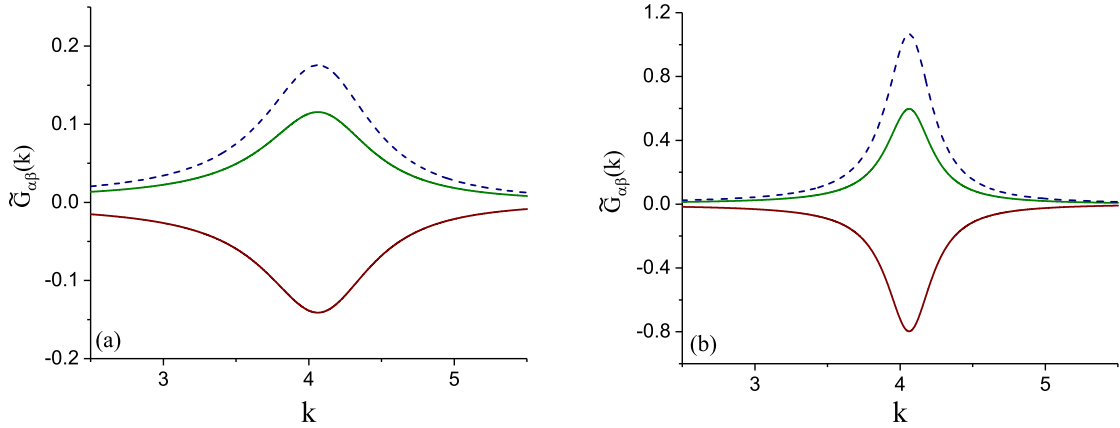
17

FIG. 11: (Colour online) Correlation functions $\tilde{G}_{\alpha,\beta}(k)$ for $\alpha = 0.6$ with the effect of fluctuations taken into account. Upper solid lines: $\tilde{G}_{11}(k)$, dashed lines: $\tilde{G}_{22}(k)$ and lower solid lines: $\tilde{G}_{12}(k)$. $T^* = 0.1$, $\zeta = 0.5$ and $c = 0.34$ (panel a), $c = 0.54$ (panel b).
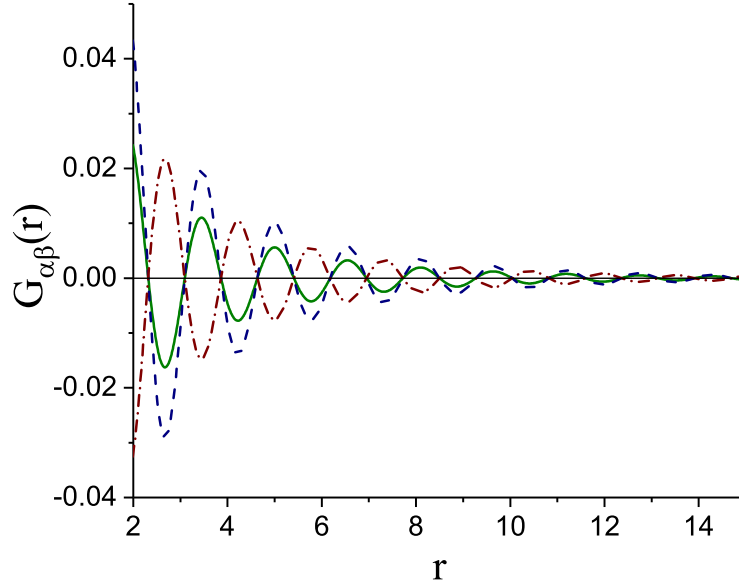

FIG. 12: (Colour online) Case $\alpha = 0.6$. Correlation functions in real space for $T^* = 0.1$, $\zeta = 0.5$ and $c = 0.54$ with the effect of fluctuations taken into account: $G_{11}(r)$ (solid line), $G_{22}(r)$ (dashed line) and $G_{12}(r)$ (dash-dotted line). r is in σ_{12} units.

of the temperature: $T^* = 0.08$ and $T^* = 0.1$. In general, the dependence of both quantities on c is similar to the behaviour observed for $\alpha = 0.8$. However, for $\alpha = 0.6$ the decay length is larger than in the case $\alpha = 0.8$ (for comparison, see also Table II where the results are shown for $\zeta = 0.4$ and 0.5).
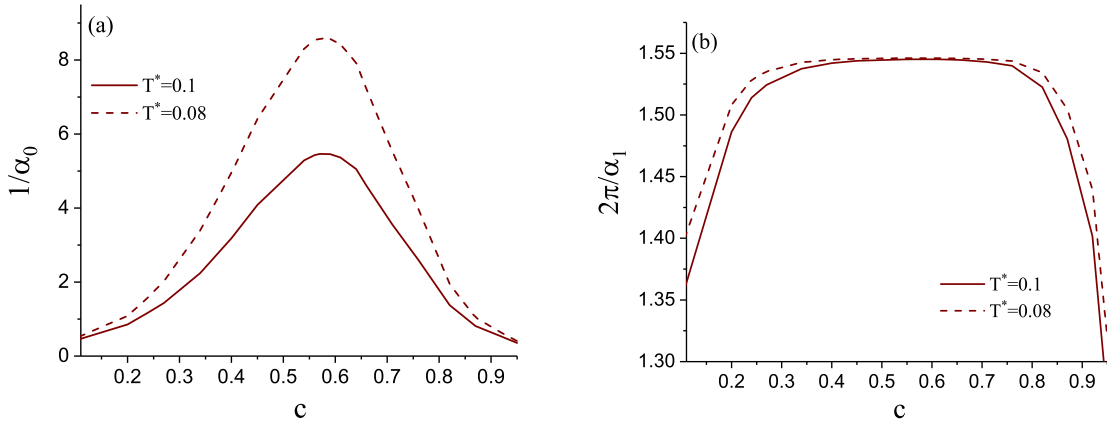
FIG. 13: The correlation length $1/\alpha_0$ (panel a) and the period of oscillations $\lambda = 2\pi/\alpha_1$ (panel b) of the correlation functions $G_{\alpha\beta}(r)$ for $\alpha = 0.6$ as functions of the concentration c for two values of temperature: $T^* = 0.08$ (dashed line) and $T^* = 0.1$ (solid line). α_0 and α_1 are in units of σ_{12}^{-1}.

2. Simulation results

The details of simulations for a binary mixture with $\alpha = 0.6$ are given in Table I (see System II).

The pair distribution functions $g_{\alpha\beta}(r)$ and a representative configuration are presented in Fig. 14 for $T^* = 0.1$, $\zeta = 0.5$ and $c = 0.54$. One can see an oscillatory decay of $g_{\alpha\beta}(r)$ with the period of damped oscillations $\lambda \approx 2\sigma_1$ that agrees with the theoretical results (see Fig. 12 noting that $\sigma_{12} \simeq 1.3\sigma_1$). The amplitude of $g_{22}(r)$ is noticeably larger than the amplitude of $g_{11}(r)$, that agrees with theoretical results for $G_{\alpha\beta}(r)$, the minimum of $g_{\alpha\alpha}(r)$ coincides with the maximum of $g_{12}(r)$, and vice versa.

One can see on the snapshot that the bigger particles are surrounded by the smaller particles, and stay apart from one another, except from very few cases. The distribution of the small particles within the attractive shell around the bigger particle is shown in Fig. 9 (panel b). The most probable number of smaller particles in the attractive shell of the big one is $N_1 = 15$, but as in the case of $\alpha = 0.8$, the fluctuations of N_1 are large.

The concentration-concentration distribution function obtained from our theory and by MC simulations for $T^* = 0.1$, $\zeta = 0.5$ and $c = 0.54$ is shown in Fig 15. We can see that the theoretical and simulation results are in reasonable agreement: in both cases the distribution function $g_{cc}(r)$ shows oscillatory decay with the same period of damped oscillations: $\lambda \approx 2\sigma_1 = 1.5\sigma_{12}$. The amplitudes are in semiquantitative agreement, but the correlation length
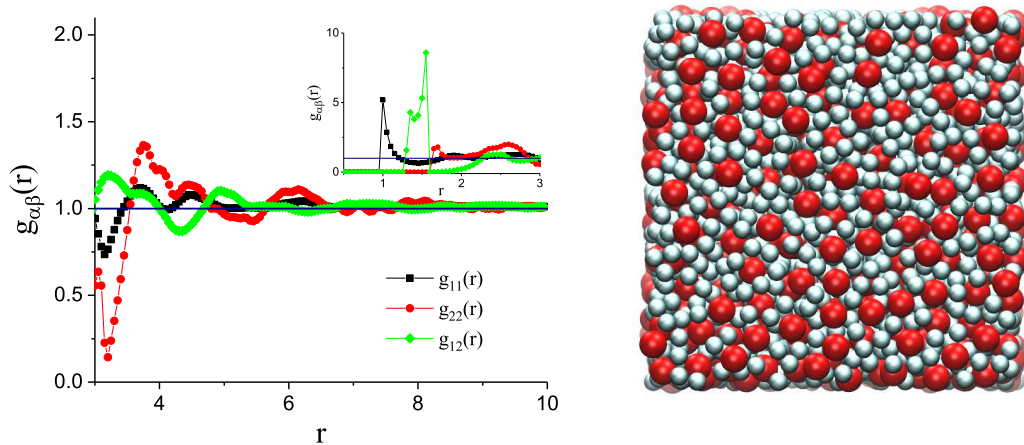
FIG. 14: (Colour online) Pair distribution functions and a representative configuration of the model with $\alpha = 0.6$ for $T^* = 0.1$, total volume fractions $\zeta = 0.5$ and concentration $c = 0.54$. r is in σ_1 units.
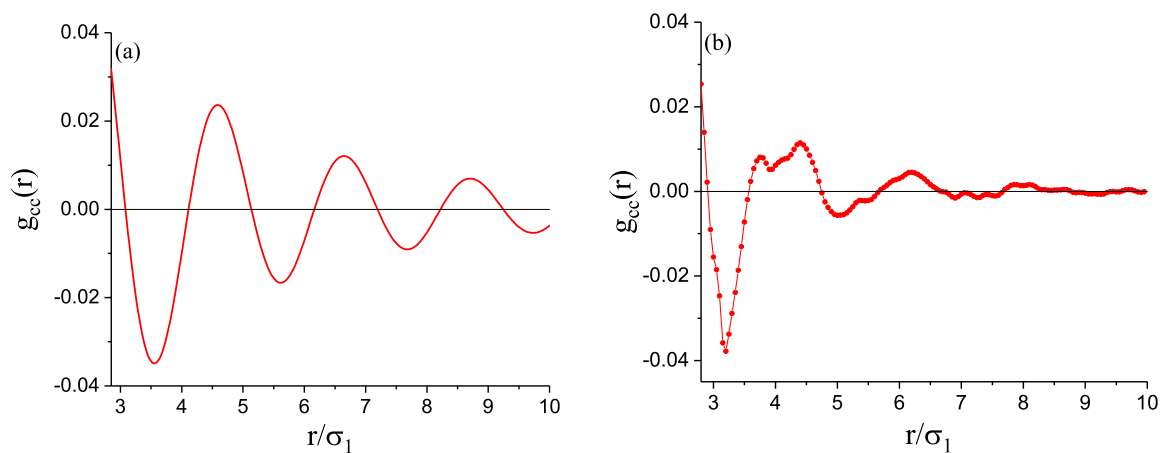
obtained in the theory is larger.

FIG. 15: (Colour online) Concentration-concentration distribution function $g_{cc}(r)$ for $\alpha = 0.6$ and for $T^* = 0.1$, $\zeta = 0.5$ and $c = 0.54$. Panel a: theoretical results, panel b: simulation results. r is in σ_1 units.

C. Case $\alpha = 0.25$

1. Theoretical results

Finally, we focus on a large size asymmetry of the particles of different species, namely, we consider a binary mixture with $\alpha = 0.25$ ($\sigma_2 = 4\sigma_1$). In this case, the MF boundaries of stability for the fixed values of concentration have the form presented in Fig. 16. As for a smaller size asymmetry, the dependence of T^* on the concentration at the fixed ζ is nonmonotonic. In addition, the form of the λ-lines changes significantly: starting from a certain value of ζ, they become almost parallel to the y-axis.
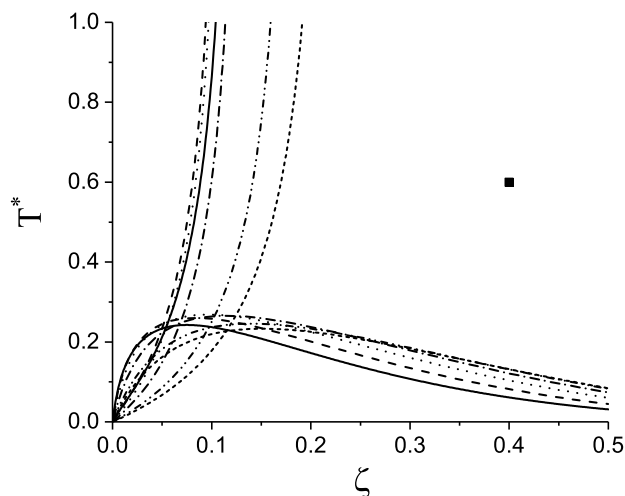

FIG. 16: Gas-liquid spinodals and λ-lines for the model (2) at $a = 1.2$ and $\alpha = 0.25$ for different values of concentration. Solid lines: $c = 0.62$ ($x = 0.025$), dashed lines: $c = 0.77$ ($x = 0.05$), dotted lines: $c = 0.88$ ($x = 0.1$), dash-dotted lines: $c = 0.94$ ($x = 0.2$), dash-dot-dotted lines: $c = 0.98$ ($x = 0.4$), and short-dashed lines: $c = 0.99$ ($x = 0.5$). The filled square denotes the thermodynamic state located below the λ-surface but above the gas-liquid spinodal (see text for more details).

We calculate the correlation functions in Fourier representation for $T^* = 0.6$, $\zeta = 0.4$ and for two values of the concentration of the big particles: $c = 0.49$ and $c = 0.67$ (the corresponding thermodynamic state is denoted by the filled square in Fig. 16). The results are presented in Fig. 17. For $c = 0.67$, the dependences of $\tilde{G}_{\alpha\beta}(k)$ on k show narrow peaks at $k = k_0$ (Fig. 17, panel b) which widen already for $c = 0.62$ and simultaneously the heights of the peaks reduce. For $c = 0.49$, the extrema of $\tilde{G}_{\alpha\beta}(k)$ become flat (Fig. 17, panel a). It should be noted that for the considered thermodynamic states, Eqs. (15)-(18) have no
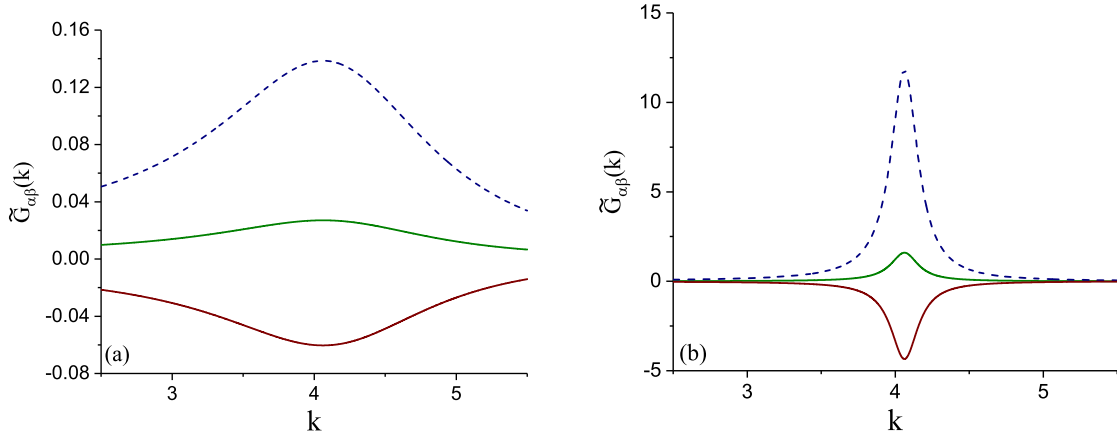
21

FIG. 17: (Colour online) Correlation functions $\tilde{G}_{\alpha,\beta}(k)$ for $\alpha = 0.25$ with the effect of fluctuations taken into account. Upper solid lines: $\tilde{G}_{11}(k)$, dashed lines: $\tilde{G}_{22}(k)$ and lower solid lines: $\tilde{G}_{12}(k)$. $T^* = 0.6$, $\zeta = 0.4$ and $c = 0.49$ (panel a), $c = 0.67$ (panel b).

solutions for $c \geq 0.7$.

In Fig. 18, the correlation functions in real space representation are presented for $T^* = 0.6$, $\zeta = 0.4$ and $c = 0.67$. As for a smaller size asymmetry, the correlation functions $G_{\alpha\beta}(r)$ have the form (32) and show exponentially damped oscillatory decay with the period of damped oscillations $\lambda \approx 1.55\sigma_{12}$. For $T^* = 0.6$, $\zeta = 0.4$ and $c = 0.67$, we have $\alpha_0\sigma_{12} \simeq 0.11$, $\alpha_1\sigma_{12} \simeq$ 4.1. The amplitudes obey the rule Eq. (33) and their values are as follows: $A_{11} \simeq 0.12$, $A_{22} \simeq 0.85$, and $A_{12} \simeq -0.32$.

In Fig. 19, the decay length α_0^{-1} and the period of damped oscillations λ are presented as functions of the concentration c for the fixed total volume fraction ($\zeta = 0.4$) and for two values of the temperature: $T^* = 0.4$ and $T^* = 0.6$. In contrast to the cases of a smaller size asymmetry, the decay length first increases very slowly on increasing the concentration and then (for $c > 0.55$) reaches its maximum very rapidly. The largest value of α_0^{-1} increases significantly with decreasing temperature. Moreover, the decay length for $\alpha = 0.25$ is much larger than in the case of smaller size asymmetry, even for the higher temperature (see the data in Table I). λ, in turn, does not exhibit a steep increase with c.
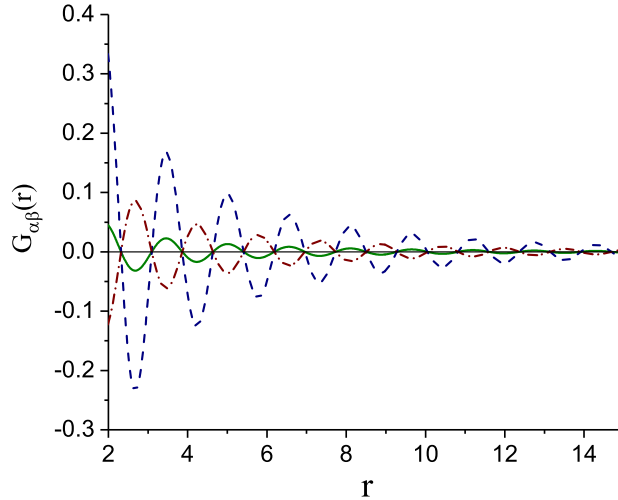
22

FIG. 18: (Colour online) Case $\alpha = 0.25$. Correlation functions in real space with the effect of fluctuations taken into account for $T^* = 0.6$, $\zeta = 0.4$ and $c = 0.67$: $\tilde{G}_{11}(k_0)$ (solid line), $\tilde{G}_{22}(k_0)$ (dashed line) and $\tilde{G}_{12}(k_0)$ (dash-dotted line). r is in σ_{12} units.
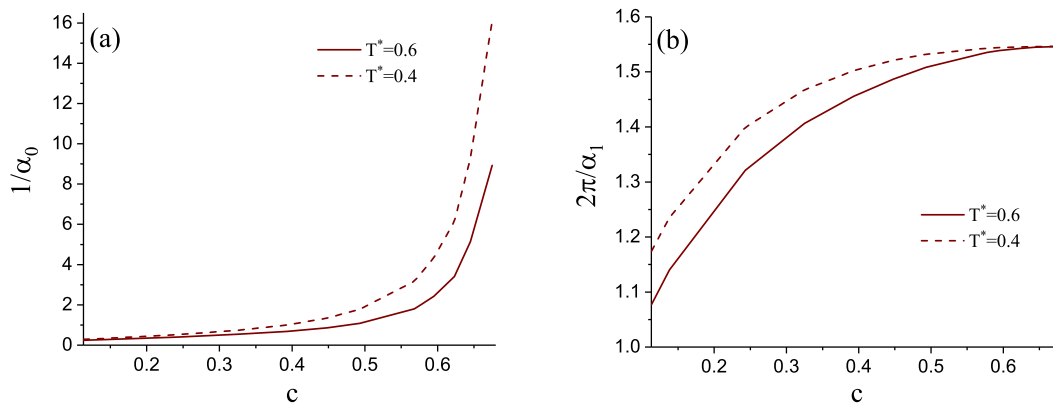

FIG. 19: The decay length α_0^{-1} (panel a) and the period of oscillations $\lambda = 2\pi/\alpha_1$ (panel b) of the correlation functions $G_{\alpha\beta}(r)$ for $\alpha = 0.25$ as functions of the concentration for two values of temperature: $T^* = 0.4$ (dashed curve) and $T^* = 0.06$ (solid curve). α_0 and α_1 are in units of σ_{12}^{-1}.

2. Simulation results

The simulations are performed for $T^* = 0.6$, $\zeta = 0.4$ and $c = 0.67$. The details of simulation are presented in Table I (System III). In this case, however, we limit ourselves to determination of the propertis of the attractive shell of the big particles. The previous cases confirm that the distribution of the particles on the mesoscopic length scale can be predicted

23

by our theory with semi-quantitative agreement with simulations. Thus, it is not necessary to determine the long-distance properties of the pair-distribution function by simulations that for large size asymmetry are much more demanding [35]. On the other hand, the short-distance structure cannot be determined by our mesoscopic theory, and this complementary information about local ordering can be obtained by our simulation procedure.
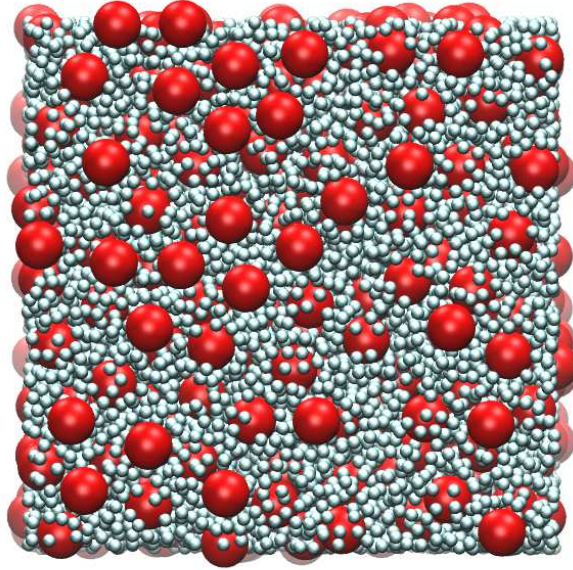

FIG. 20: (Colour online) A representative configuration of the model with $\alpha = 0.25$ for $T^* = 0.6$, total volume fraction $\zeta = 0.4$ and concentration $c = 0.67$.

In Fig. 20, a representative configuration is shown. As it is seen from the snapshot, the big particles are surrounded by the small particles, and have a strong tendency to the periodic ordering. This is also supported by the histogram in Fig. 9 (panel c). As one can see, $P(N_1)$ is quite narrow in contrast to the previously considered cases. The ratio between the standard deviation and the average number of the 'adsorbed' particles is quite small, and can be estimated as $\sim 5\%$. The theoretical results show quite large correlation length for the considered thermodynamic state. We conclude that the periodic ordering on the length scale of σ_2, and the ordering near the surface of the big particles (meaning large number of the small particles in the attractive shell and small fluctuations of this number) go together.

V.   SUMMARY AND CONCLUSIONS

We have studied binary mixtures with effective interactions between the particles that favour nearest-neighbours of different kind. At low temperature, such interactions lead to a periodic structure with alternating particles of the first and the second component. At higher T the crystal melts, but a competition between the ordering effect of energy and disordering effect of entropy leads to local periodic order. Our aim was determination of the effect of size asymmetry of the particles of the two species on this local order.

We have calculated correlation functions for small, medium and large size asymmetry within the mesoscopic DFT developed in Ref.[24, 25], at the lowest nontrivial order beyond MF. Our results were favourably compared with MC simulations on a semiquantitative level. In addition, the simulations allowed us to determine the distribution of the small particles in the attractive shell of the bigger ones.

We have found that for all considered size ratios α the correlation functions show exponentially damped oscillations, with the maxima of the correlation function for like species that coincide with the minima of the correlation function for different species. The range and amplitude of the correlations increase with decreasing T and/or increasing total volume fraction of the particles. In each considered system, the period $2\pi/\alpha_1$ of the damped oscillations is almost independent of their relative volume fraction of the large particles, $c = \zeta_2/\zeta$, as long as the correlation length is larger than 1 (in σ_{12} units). Moreover, α_1 is very close to the wave-number corresponding to the first maximum of the interaction between different species in Fourier representation. Only for the correlation length $1/\alpha_0 < 1$, i.e. too small for formation of the periodic structure on the mesoscopic length scale, the period of the damped oscillations decreases. Another common feature of all the considered cases is the fact that the correlations between the bigger particles are the strongest for a large interval of their relative volume fraction c. Only for c smaller than a value depending on α, the correlations between the smaller particles are larger. This value of c, however, decreases rapidly with decreasing α (increasing size ratio).

In addition to the above similarities, there are significant differences between the properties of the systems with different size ratio α. First of all, correlations increase significantly with increasing size ratio, and are much stronger in the case of $\alpha = 0.25$ than for $\alpha \geq 0.6$. The amplitude and range of correlations in the case of large size-asymmetry are significantly

25

larger even at T much higher than in the system with moderate size ratio. The dependence of the local order on c in the system with large size-ratio is qualitatively different than in the systems with moderate or small size asymmetry. In the latter two cases, the correlation length takes a pronounced maximum for comparable volume fractions of the two species. With increasing size asymmetry, the maximum of the correlation length moves to a larger volume fraction of the bigger particles. The difference between the amplitudes of the correlation function between the big particles and the remaining correlation functions increases with increasing size asymmetry too. For $\alpha = 0.25$, however, the correlation length is very small for small c, and increases very slowly with c for $c < 0.5$. For $c > 0.5$ a rapid increase to large numbers occurs, and both $1/\alpha_0$ and $2\pi/\alpha_1$ are monotonic functions of c, in contrast to the previous two cases. Moreover, the magnitude of the correlations between the big particles becomes much larger than the magnitude of the remaining correlations for all values of c corresponding to $1/\alpha_0 > 1$.

The stronger ordering on the mesoscopic length scale is accompanied by stronger ordering in the attractive shell of the big particles. For $\alpha = 0.8$ and $\alpha = 0.6$, the average number of the smaller particles located in the attractive shell of the big particle is 8 and 15, respectively. This number, however, fluctuates strongly, and in the considered thermodynamic state, the ratio between the standard deviation and the average number of particles can be estimated as $\sim 25\%$ and $\sim 20\%$, respectively. On the other hand, for $\alpha = 0.25$ and the considered thermodynamic state, the average number of the small particles inside the attractive shell of the big one is 37.5, and the ratio between the standard deviation and the average number of particles can be estimated as $\sim 5\%$. Notably, the temperature in this case is much higher than in the above two cases.

Our results show that for all considered cases, the bigger particles are distributed much more uniformly than in the random distribution. Even though the long-range order is lacking, the distance between the nearest-neighbours of the same kind is approximately the same, and the big particles are separated by the small ones (see Fig.20). In some way our models resemble hyperuniform systems [36, 37]. Our results suggest that the larger is the

size ratio, the more uniformly are distributed the larger particles.

---

[1] P. C. Royall, M. E. Leunissen, A.-P. Hynninen, M. Dijkstra, and A. van Blaaderen, *J. Chem. Phys.* **124**, 244706 (2006).

[2] M. Leunissen, C. Christova, A.-P. Hynninen, C. Royal, A. Campbell, A. Imhof, M. Dijkstra, R. van Roji, and A. van Blaaderen, *Nature* **437**, 235 (2005).

[3] A. P. Hynninen, M. E. Leunissen, A. van Blaaderen, and M. Dijkstra, *Phys. Rev. Lett.* **96**, 018303 (2006).

[4] K. Shimizu, M. Tariq, A. A. Freitas, A. A. H. Pádua, and J. N. C. Lopes, *J. Braz. Chem. Soc.* **27**, 349 (2015).

[5] F. H. Stillinger and R. Lovett, *J. Chem. Phys.* **48**, 3858 (1968).

[6] R. L. de Carvalho and R. Evans, *Mol. Phys* **83**, 619 (1994).

[7] A. Ciach and G. Stell, *Int.J. Mod. Phys. B* **19**, 3309 (2005).

[8] A. Ciach, W. T. Gozdz, and G. Stell, *J. Phys.: Condens. Matter* **18**, 1629 (2006).

[9] A. Ciach and O. Patsahan, *Phys. Rev. E* **74**, 021508 (2006).

[10] O. Patsahan and A. Ciach, *Phys. Rev. E* **86**, 031504 (2012).

[11] O. Patsahan and A. Ciach, *J. Phys.: Condens. Matter* **19**, 236203 (2007).

[12] A. M. Smith, A. A. Lee, and S. Perkin, *J. Phys. Chem. Lett.* **7**, 2157 (2016).

[13] M. V. Fedorov and A. A. Kornyshev, *J. Phys. Chem. B* **112**, 11868 (2008).

[14] M. V. Fedorov and A. A. Kornyshev, *Chem. Rev.* **114**, 2978 (2014).

[15] J. M. Otero-Mato, H. Montes-Campos, O. Cabeza, D. Diddens, A. Ciach, L. J. Gallego, and L. M. Varela, *Phys. Chem. Chem. Phys.* **20**, 30412 (2018).

[16] A. Ciach, *J. Mol. Liq.* **270**, 138 (2018).

[17] H. Montes-Campos, J. M. Otero-Mato, T. Méndez-Morales, O. Cabeza, L. J. Gallego, A. Ciach, and L. M. Varela, *Phys. Chem. Chem. Phys.* **19**, 24505 (2017).

[18] M. Bradley, A. M. Lazim, and J. Eastoe, *Polymers* **3**, 1036 (2011).

[19] P. Attard, *Phys. Rev. E* **48**, 3604 (1993).

[20] R. Evans, *Adv. Phys.* **28**, 143 (1979).

[21] A. Ciach, *Soft Matter* **14**, 5497 (2018).

[22] A. Ciach, W. T. Góźdź, and R.Evans, *J. Chem. Phys.* **118**, 3702 (2003).

[23] A. Ciach, W. T. Góźdź, and G. Stell, *Phys. Rev. E* **75**, 051505 (2007).

[24] A. Ciach, *Mol. Phys* **109**, 1101 (2011).

[25] A. Ciach, O. Patsahan, and A. Meyra, *Condens. Matter Phys.* **23**, 23601 (2020).

[26] G. Orkoulas and A. Z. Panagiotopoulos, *J. Chem. Phys.* **110**, 1581 (1999).

[27] Q. Yan and J. J. de Pablo, *J. Chem. Phys.* **111**, 9509 (1999).

[28] D. Cheong and A. Panagiotopoulos, *J. Chem. Phys.* **119**, 8526 (2003).

[29] A. Ciach, J. Pękalski, and W. T. Góźdź, *Soft Matter* **9**, 6301 (2013).

[30] S. A. Brazovskii, *Sov. Phys. JETP* **41**, 85 (1975).

[31] A. Ciach and O. Patsahan, *Condens. Matter Phys.* **15**, 23604 (2012).

[32] G. Mansoori, N. F. Carnahan, K. E. Starling, and J. T. W. Leland, *J. Chem. Phys.* **54**, 1523 (1971).

[33] R. Evans, R. L. de Carvalho, J. R. Henderson, and D. C. Hoyle, *J. Chem. Phys.* **100**, 591 (1994).

[34] N. H. March and M. P. Tosi, *Atomic Dynamics in Liquids* (Macmillan Education, UK, 1976).

[35] D. J. Ashton, J. Liu, E. Luijten, and N. Wilding, *J. Chem. Phys.* **133**, 194102 (2010).

[36] S. Torquato and F. H. Stillinger, *Phys. Rev. E* **68**, 041113 (2003).

[37] A. G. Meyra, G. J. Zarragoicoechea, A. L. Maltz, E. Lomba, and S. Torquato, *Phys. Rev. E* **100**, 022107 (2019).